Received 14 March 2024; accepted 17 April 2024. Date of publication 22 April 2024; date of current version 6 August 2024.

Digital Object Identifier 10.1109/OJAP.2024.3391799

Synthesis and Design of 3-D Microwave Absorber With 70° Angular Stability for C-Band and X-Band

TIAN-XI FENG [1] (Member, IEEE), LEI ZHU [2,3] (Fellow, IEEE), AND HUI LI [1] (Senior Member, IEEE)

(Invited Paper)

[1]School of Information and Communication Engineering, Dalian University of Technology, Dalian 116024, China

[2]State Key Laboratory of Internet of Things for Smart City, University of Macau, Macau, China

[3]Department of Electrical and Computer Engineering, Faculty of Science and Technology, University of Macau, Macau, China

CORRESPONDING AUTHOR: L. ZHU (e-mail: leizhu@um.edu.mo)

This work was supported in part by the Fundamental Research Funds for the Central Universities under Grant DUT24RC(3)004; in part by the National Natural Science Foundation of China under General Program under Grant 61971475; in part by the Macao Science and Technology Development Fund under FDCT Research under Grant 0085/2020/AMJ, Grant 0080/2021/A2, and Grant 0075/2023/RIA2; and in part by the University of Macau under Grant CPG2024-00014-FST and Grant MYRG-GRG2023-00031-FST-UMDF.

ABSTRACT This article presents the synthesis and design of 3-D microwave absorber with 70° angular stability for C-band and X-band. The operating principle is firstly investigated, where the absorber is considered as an energy convertor. With the help of our proposed universal equivalent transmission line (TL) model, the absorptive performance can be accordingly synthesized. Then, a design method for efficient absorption under large angles is presented. By selecting a proper synthesized angle (SA), the angular stability can be effectively improved. After that, the prototype with 70° angular stability is designed as an example with structural realization and practical implementation. Measurements agree well with synthesized and simulated results, successfully verifying the proposed design method. For specific C-band and X-band applications, the measured average absorption ratios (ARs) under normal incidence, 45° incidence, and 70° incidence are 94.2%, 94.0%, and 92.3%. Minimum measured ARs within the operating bandwidth are 88.4%, 81.5%, and 82.0% for normal, 45°, and 70° incidences. Besides, the proposed absorber element owns the advantage of simple structure with only one resistor. Such a class of microwave absorber is a potential candidate for wide coverage electromagnetic absorption.

INDEX TERMS 3-D microwave absorber, angular stability, synthesis and design, universal equivalent transmission line model.

I. INTRODUCTION

MICROWAVE absorbers have attracted widespread attention in the research field of electromagnetic scattering, due to their essential role in radar cross section (RCS) reduction, electromagnetic interference (EMI) shielding, and anechoic chambers applications [1]. As one of the most significant performances, a larger angular stability is highly preferred for wide coverage of electromagnetic absorption.

During the past few years, great effort has been made to develop wide-angle absorbers. Different resistive or absorptive material-based designs were reported with large angular stability. In [2], octagonal ring-shaped resistive patches were used to obtain a metamaterial absorber with interference theory. The graphene-based structures were utilized in [3] and [4] for large-angle designs. In [5] and [6], the water-based and biomass-based absorbers were presented with enhanced absorption performance. The indium tin oxide (ITO) film was employed in [7] and [8] to improve the wide-angle performance. In [9], the spatial lossy transmission line was proposed to realize a wide absorption band while maintaining a large oblique incident angle stability. The ink-based resistive layer was used in [10] to cope with the wideband RCS reduction under a planar structure. In [11], polycarbonate substrate was coated with gold films for the broadband absorber with optical transparency. Using ruthenium oxide on a low-temperature co-fired ceramic

substrate, an ultrathin single-layer broadband absorber was presented in [12].

In addition to applying resistive materials, lumped loading is also a popular method to design microwave absorber with improved performance. A lump circuit modeling was proposed in [13] to analyze and design a flexible structure for conformal electromagnetic absorbers. In [14], a wideband absorber was presented based on spoof surface plasmon polariton to obtain a high angular stability. By integrating electric resonances and magnetic resonances, a wideband absorber with wide-angle response was reported in [15]. In [16], a type of frequency selective surface (FSS) was introduced in the bottom layer to increase the absorption bandwidth. A single-layer impedance-well passive absorber was put forward in [17] with enhanced absorption bandwidth approaching the Rozanov thickness limit for passive absorbers. In [18], a pair of rectangular patches and a rectangular loop embedded with four resistors were utilized to design a broadband microwave absorber operating at an oblique angle of 75°. A wideband circuit analog absorber was realized in [19] based on the concept of multiple resonances.

More than the above-mentioned methods, structural deformation is able to significantly improve angular stability as well. In [20], the conformal broadband metamaterial was used to put forward a microwave absorber with high angular stability. The wide-angle electromagnetic absorption was addressed in a dynamically controllable manner via a reconfigurable origami-based metamaterial [21]. The 3-D origami absorber with four normal vectors provided an effective approach to prevent the deterioration of absorption in a wide-angle range. In [22], the performance under the oblique incidence over wide-angle and wideband was improved by rotating the FSS in 3-D planes through various rotation schemes. However, for these existing works, there is no universal synthetic design method that can provide both predicted wide-angle and wideband performance simultaneously.

In this article, we present the synthesis and design of 3-D microwave absorber with specific performance, such as 70° angular stability within C-band and X-band. The operating principle is firstly investigated, where the absorber is considered as an energy convertor. Using our established universal equivalent transmission line (TL) model, the absorptive performance can be accordingly synthesized. Then, we propose a design method to realize efficient absorption under large angles. Most importantly, a synthesized angle (SA) is properly selected to effectively improve the angular stability. After that, a prototype is designed for the 70° angular stability as an example from structural realization to practical implementation. Measurements agree well with synthesized and simulated results, which successfully validates the proposed design method. For given operating frequency in C-band and X-band, the measured average absorption ratios (ARs) under normal incidence, 45° incidence, and 70° incidence are 94.2%, 94.0%, and 92.3%. Minimum measured ARs within the operating bandwidth are 88.4%, 81.5%, and 82.0% for normal, 45°, and 70° incidences. Additionally, the proposed absorber element possesses the advancement of simple structure which needs only one resistor. Therefore, such a type of microwave absorber is indeed a promising candidate for wide coverage electromagnetic absorption. The main novelties and contributions are summarized as follows:

a) Based on the established equivalent TL model, it is easy to synthetic design the Chebyshev absorptive response with different orders and symmetries.
b) By employing a synthesized angle of 45° rather than the traditional 0°, the angle coverage within operating bands is significantly improved to 70° with high efficiency.
c) The proposed absorber element only applies one piece of substrate and one resistor, avoiding the complex structure caused by multi-layered substrates and multiple resistors.

II. OPERATING PRINCIPLE

The operating principle of the proposed absorber is depicted in Fig. 1. The electromagnetic wave in free space flows to the proposed conversion structure, which can be analyzed and designed using microwave circuit theory. Then, the input energy is transformed into thermal energy by the absorption structure (here, a resistor). During this process, the most crucial steps are how to establish a suitable circuit model and how to implement this model under a simple structure.

With regard to the first vital step, a universal equivalent TL model is constructed for the conversion structure, as shown in Fig. 1. A pair of edge-connecting lines are named as TL_a and TL_d. Two sets of shunt short-ended stubs are denoted as TL_b and TL_c. Several sections of middle connecting lines are represented as TL_1, TL_2, ..., TL_i, ..., TL_{n-1}, and TL_n. The impedance of spatial wave is Z_0, the input impedance is Z_{in}, and the loaded resistance is Z_R. In this model, all the TLs are of the same length of quarter wavelength at the desired center frequency. Due to the fact that the characteristic impedance of each TL is not limited by any condition, this model can perform as a symmetric or asymmetric model according to the desired response. Moreover, different numbers of middle connecting lines result in circuit property with different orders. Thus, the proposed universal equivalent model owns the capability of converting the input energy under arbitrary order and arbitrary symmetry.

$$\begin{bmatrix} A & B \\ C & D \end{bmatrix}_{\text{ele.}} = \begin{bmatrix} A & B \\ C & D \end{bmatrix}_a \begin{bmatrix} A & B \\ C & D \end{bmatrix}_b \begin{bmatrix} A & B \\ C & D \end{bmatrix}_1 \begin{bmatrix} A & B \\ C & D \end{bmatrix}_2 \cdots \begin{bmatrix} A & B \\ C & D \end{bmatrix}_i \cdots \begin{bmatrix} A & B \\ C & D \end{bmatrix}_{n-1} \begin{bmatrix} A & B \\ C & D \end{bmatrix}_n \begin{bmatrix} A & B \\ C & D \end{bmatrix}_c \begin{bmatrix} A & B \\ C & D \end{bmatrix}_d \quad (1)$$

According to our established model, the ABCD matrix of the proposed element is calculated as (1) [23], [24]. In this way,

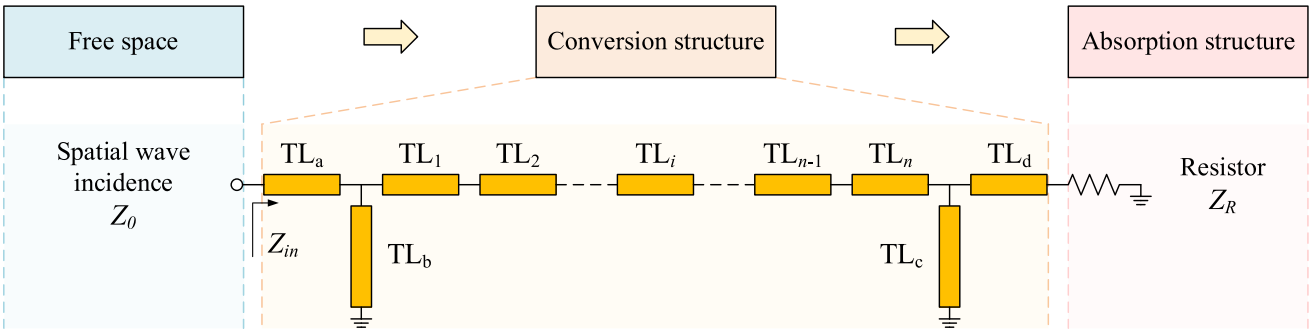

FIGURE 1. Operating principle and universal equivalent transmission line model of the proposed 3-D absorber element.

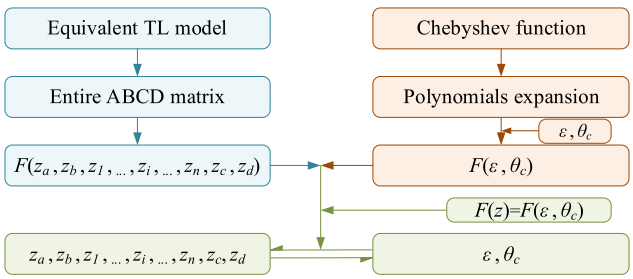

FIGURE 2. Summary of the synthetic procedure for the proposed universal model.

the characteristic function can be derived using impedances in this model as [25], [26], [27]

$$F = f\left(\frac{1}{\sin\theta}, cos\theta, z_a, z_b, z_1, \ldots, z_i, \ldots, z_n, z_c, z_d\right) \quad (2)$$

Combining the Chebyshev polynomials

$$\varepsilon \cos(p\varphi + q\xi) = f\left(\frac{1}{\sin\theta}, cos\theta, \varepsilon, \alpha\right) \quad (3)$$

we can obtain the relationship between characteristic impedances (in the equivalent model) and expected responses (in Chebyshev polynomials). Here, z denotes the normalized characteristic impedance, ε is related to the maximum in-band reflection coefficient Γ, p (and q) is a positive integer, and α is determined by the lower cutoff frequency f_c. The above synthetic procedure can be summarized as shown in Fig. 2:

a) Construct an equivalent TL model and calculate the entire ABCD matrix to obtain the characteristic function. Here, the elements in the ABCD matrix include the characteristic impedance of each transmission line;

b) Properly select and expand the Chebyshev function according to the characteristic function, where the Chebyshev function contains information about the S-parameters;

c) By equating the characteristic function with the Chebyshev function, the relationship between the equivalent TL model and S-parameters (expected performance) can be obtained.

Since the key elements in our equivalent TL model are characteristic impedance and electrical length, the characteristic impedance for each section of transmission lines can be easily calculated based on the expected performance.

Without loss of generality, we take Z_R=Z_{in}, n=2 as an example. Thus, we have

$$F = j\left(k_1\frac{\cos^5\theta}{\sin\theta} + k_2\frac{\cos^3\theta}{\sin\theta} + k_3\frac{\cos\theta}{\sin\theta}\right) + k_4\cos^4\theta + k_5\cos^2\theta + k_6 \quad (4)$$

All the coefficients of k are given in the appendix. Accordingly,

$$\varepsilon\cos(4\varphi + \xi) = j\left(K_1\frac{\cos^5\theta}{\sin\theta} + K_2\frac{\cos^3\theta}{\sin\theta} + K_3\frac{\cos\theta}{\sin\theta}\right) \quad (5)$$

The coefficients of K_1, K_2, and K_3 are as follows

$$\begin{cases} K_1 = \varepsilon\left(8\alpha^5 + 8\alpha^4\sqrt{\alpha^2-1}\right) \\ K_2 = \varepsilon\left(-12\alpha^3 - 8\alpha^2\sqrt{\alpha^2-1}\right) \\ K_3 = \varepsilon\left(4\alpha + \sqrt{\alpha^2-1}\right) \end{cases} \quad (6)$$

For (4) and (5), the following equations must be satisfied

$$k_1 = K_1, k_2 = K_2, k_3 = K_3, k_4 = k_5 = k_6 = 0 \quad (7)$$

After these calculations, each characteristic impedance is determined by the given conversion response. In other words, the desired performance can be theoretically synthesized by conducting the above procedure.

Based on the foregoing analysis, we further present a novel design method for large angular stability. A highly significant parameter of the incident angle θ_{in} is taken into consideration at the very beginning of designing a conversion structure. The incident angle prominently affects the input impedance, which is always overlooked in traditional works. Here, the input impedance of practical incidence is given by [28], [29]

$$\begin{cases} Z_{in,TM}^{inc.} = Z_0\cos\theta_{in}, & \text{TM} - \text{pol.} \\ Z_{in,TE}^{inc.} = \frac{Z_0}{\cos\theta_{in}}, & \text{TE} - \text{pol.} \end{cases} \quad (8)$$

For traditional works, the element structure is designed under θ_{in}=0° (normal incidence). Due to the huge change in input impedance, the impedance mismatching under

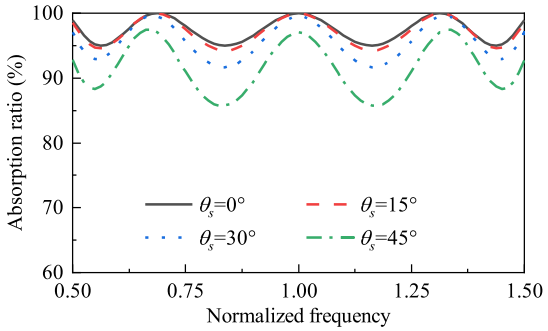

FIGURE 3. Absorption ratios with different synthesized angles under normal incidence.

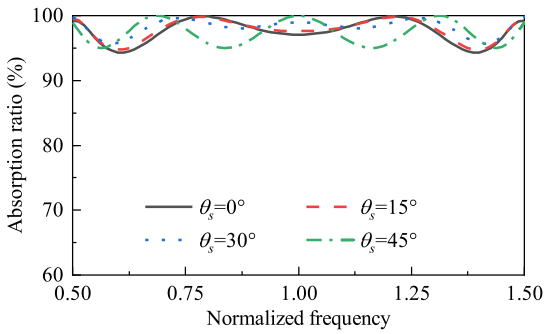

FIGURE 4. Absorption ratios with different synthesized angles under 45° incidence.

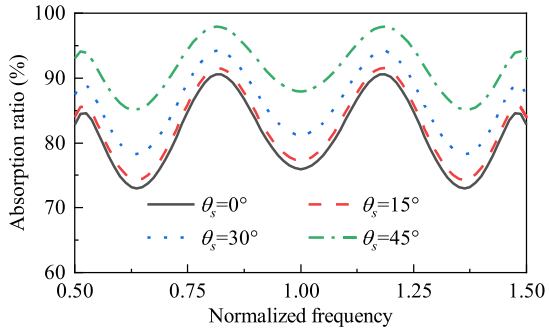

FIGURE 5. Absorption ratios with different synthesized angles under 70° incidence.

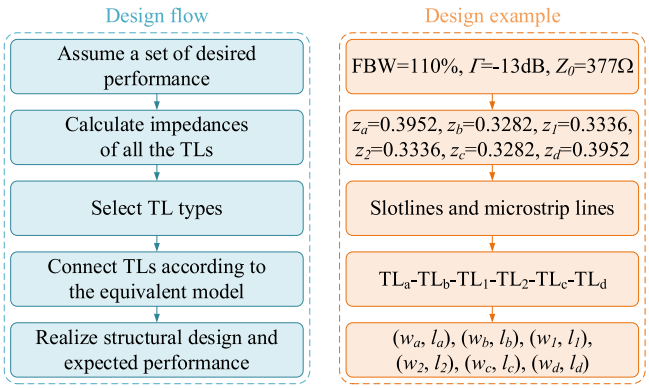

FIGURE 6. Design flow and design example of the proposed method.

oblique incidence results in obvious deterioration of element performance compared with that under normal incidence.

On the contrary, in this article, we select a synthesized angle θ_s to replace the conventional default of 0° during the design procedure, where

$$\begin{cases} Z_{in,TM}^{syn.} = Z_0 \cos\theta_{s,TM} = Z_{R,TM} \ , \ \text{TM}-\text{pol.} \\ Z_{in,TE}^{syn.} = Z_0/\cos\theta_{s,TE} = Z_{R,\text{TE}} \ , \ \text{TE}-\text{pol.} \end{cases} \tag{9}$$

In this way, the expected response will be realized when the actual incident angle is equal to the theoretical synthesized angle, which is $\theta_{in} = \theta_s$. Therefore, an appropriately selected synthesized angle is of great significance for obtaining the desired angular stability. Herein, considering a TM-polarized example where the fractional bandwidth (FBW) is 110% and $\Gamma = -13$dB, the synthesized absorption ratios (ARs) with different θ_s are shown in Fig. 3 to Fig. 5. Under normal incidence, when θ_s is 0°, as shown in Fig. 3, the AR shows the highest value as the normalized frequency increases from 0.5 to 1.5. In this case, for $\theta_s = 45°$, the AR results of higher than 85.7% is still obtained. Under 45° incidence in Fig. 4, all AR curves show high values of larger than 94%. For the most critical 70° incidence in Fig. 5, when θ_s is 45°, the AR curve attains the highest one with the minimum value of 85.1%. In this case, traditional design with $\theta_s = 0°$ only realizes a minimum AR of 73% from ideal calculations. Therefore, the proposed design method can theoretically obtain a stable AR result of higher than 85.1% within the entire desired operating bandwidth. It is worth noting that the above methods and conclusions are also applicable to TE-polarized incident wave absorption.

III. ABSORBER DESIGN AND IMPLEMENTATION

To verify the proposed method in Section II, a prototype is practically designed and implemented in this section. In order to provide a clear illustration of the design process, Fig. 6 shows the design flow and design example of the proposed method. The complete design flow can be divided into five steps:

a) Assume a set of desired absorption performance according to the given target requirements;
b) Calculate the characteristic impedances of all the TLs using the synthetic design method in Section II;
c) Choose the appropriate types of TL, taking into account both impedance and structure features;
d) Connect all the TLs corresponding with the equivalent TL model. Transitions need to be designed between different types of TLs;
e) If necessary, optimize the entire structure to ultimately obtain the expected performance.

Following the above design flow, a design example is practically implemented:

a) In order to realize the 70° coverage for C-band and X-band, we set the performance to FBW = 110%, $\Gamma = -13$dB, $Z_0 = 377$Ohm, and $\theta_s = 45°$;

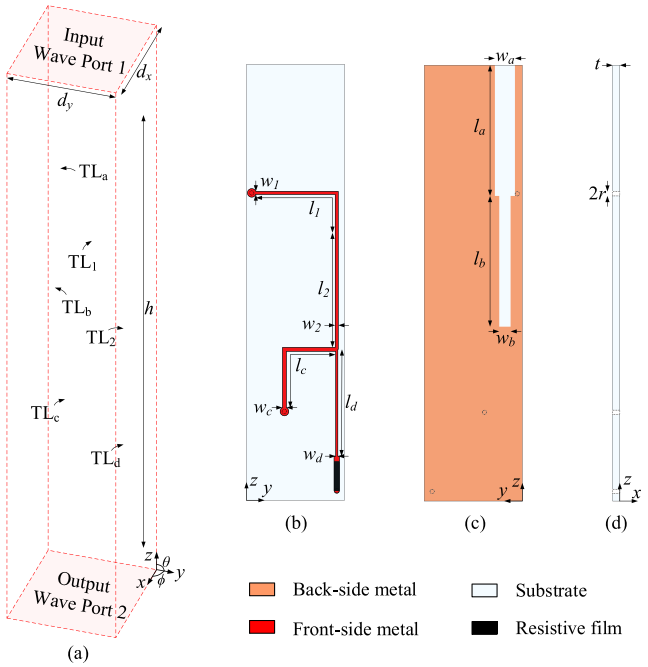

FIGURE 7. Element configuration of the proposed 3-D absorber. (a) Overall view with periodic boundary condition. (b) Front-side metal and resistive film. (c) Back-side metal. (d) Side view.

b) The characteristic impedances are calculated as $z_a = 0.3952$, $z_b = 0.3282$, $z_1 = 0.3336$, $z_2 = 0.3336$, $z_c = 0.3282$, and $z_d = 0.3952$;
c) Choose slotlines and microstrip lines to design the element structure. Two sections of slotlines (or microstrip lines) can be directly connected to each other. The transition between slotlines and microstrip lines is realized through a short-circuited structure;
d) The first two sections of TLs (TL_a and TL_b) are slotlines, while the other four sections of TLs (TL_1, TL_2, TL_c, and TL_d) are microstrip lines. TL_b and TL_c are connected to the ground in parallel;
e) The corresponding sizes of microstrip lines and slotlines can be easily obtained by using TL calculator and periodic slotline simulations, respectively. The final dimensions of the entire element are optimized as $d_x = 4.5$, $d_y = 4.5$, $h = 20$, $t = 1$, $w_a = 0.92$, $l_a = 6$, $w_b = 0.52$, $l_b = 6$, $w_1 = 0.14$, $l_1 = 5.54$, $w_2 = 0.14$, $l_2 = 5.54$, $w_c = 0.18$, $l_c = 5.25$, $w_d = 0.1$, $l_d = 4.9$, $r = 0.1$. (unit: mm)

Here, the reasons for using different types of transmission lines can be explained from two aspects: 1) slotlines are employed to achieve efficient energy conversion from spatial waves in free space to guided waves in transmission lines, and 2) microstrip lines are used to realize the absorptive circuit where a resistive load is connected in series at the end of the last transmission line.

The element configuration of the proposed absorber design is shown in Fig. 7. From the overall view in Fig. 7(a),

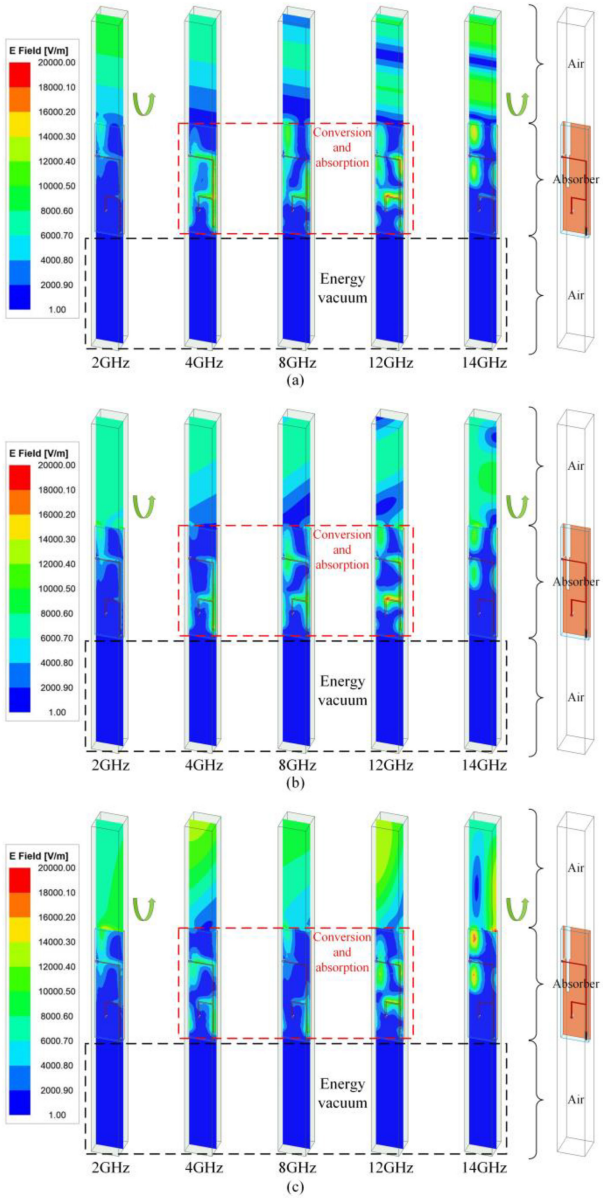

FIGURE 8. Electric field distribution for the proposed absorber element under (a) normal incidence, (b) 45° incidence, and (c) 70° incidence.

the single-layered structure is surrounded by the periodic boundary condition. Two sections of slotlines (TL_a and TL_b) are etched on the backside ground, while four sections of microstrip lines (TL_1, TL_2, TL_c, and TL_d) are printed on the front side. The loaded resistor is made by the resistive film from Ohmega (50Ohm/square) and connected to the backside ground via a shorting pin. In order to realize a good structural strength under effective cost, the FR4 substrate (relative permittivity of 4.4, loss tangent of 0.0166) is employed in this work. Fig. 7(b) shows the detailed view for microstrip lines and resistive film, where the bent transmission lines are for a compact element size.

To clearer display the absorption performance, Fig. 8 shows electric field distribution of the proposed absorber

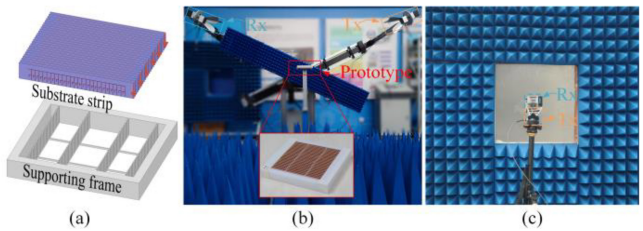

FIGURE 9. (a) Assembly process of the fabricated prototype, (b) reflectivity testing system, and (c) transmission testing system.

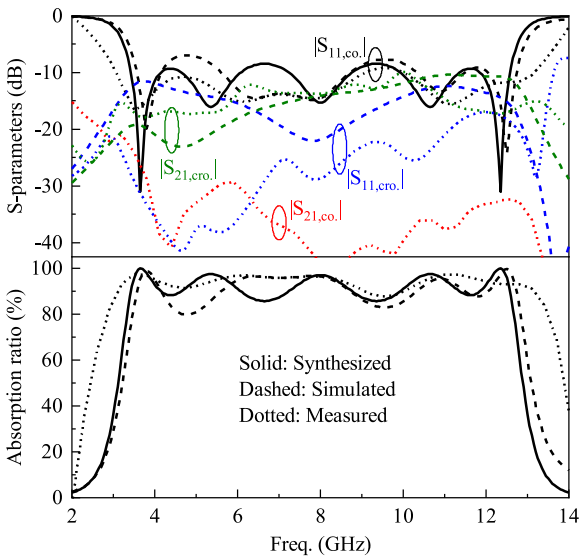

FIGURE 10. Synthetizations, simulations, and measurements of S-parameters and absorption ratios for the proposed design under normal incidence.

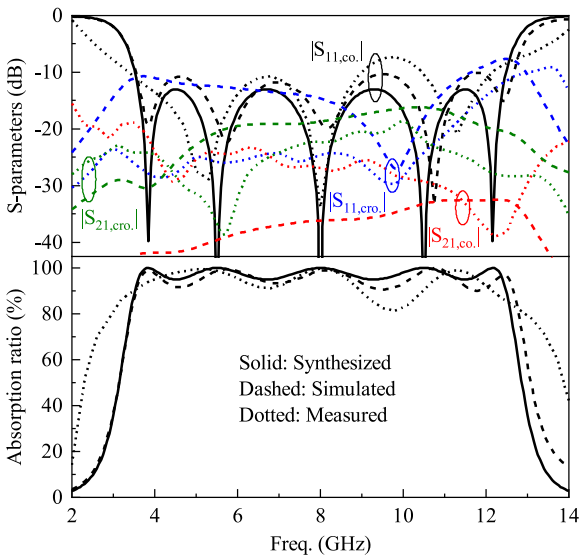

FIGURE 11. Synthetizations, simulations, and measurements of S-parameters and absorption ratios for the proposed design under 45° incidence.

element under different incidences. As seen in Fig. 8(a), for out-of-band frequencies (2GHz on the left and 14GHz on the right), the incident wave is reflected back to the upper free

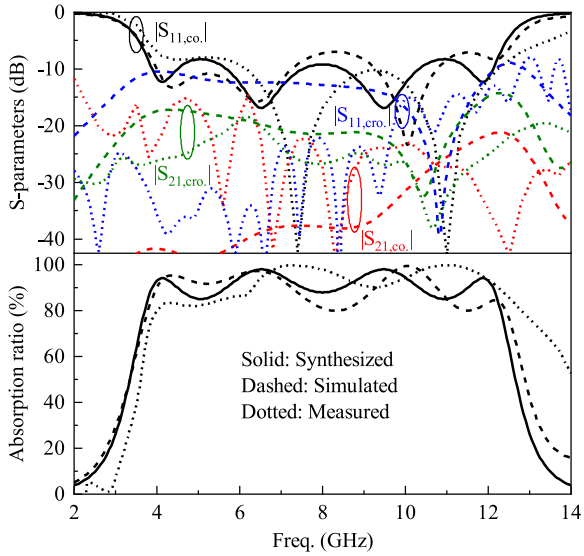

FIGURE 12. Synthetizations, simulations, and measurements of S-parameters and absorption ratios for the proposed design under 70° incidence.

TABLE 1. Performance summary of the proposed absorber.

	Bandwidth			Average AR		
	0°	45°	70°	0°	45°	70°
Synthesis	116.2%	113.7%	106.2%	92.1%	97.2%	91.3%
Simulation	114.1%	114.8%	106.1%	91.0%	95.0%	90.0%
Measurement	128.8%	120.0%	103.9%	93.5%	92.9%	92.0%

space. Meanwhile, the incidence within operating bandwidth (4GHz, 8GHz, and 12GHz in the middle) is absorbed by the proposed structure. The conversion and absorption can be well defined from the electric field distribution. In this way, the energy vacuum can be realized in the free space below the proposed element. Regarding oblique incidences in Fig. 8(b) and Fig. 8(c), similar phenomena occur as well, which further validates the wide-angle performance.

This designed absorber is fabricated and tested, as shown in Fig. 9. In order to guarantee the proper element distances and attain a durable prototype, a supporting frame is made of photosensitive resin and applied for the actual absorber with 25×25 elements, as shown in Fig. 9(a). Then, 25 pieces of substrate strip are inserted into the supporting frame. In Fig. 9(b), the bow-shaped reflectivity testing system is used to obtain the accurate reflection coefficients. The transmitting and receiving horns (Tx and Rx) are located on two swinging arms, and gradual rotation on the same radius arc trajectory to realize reflectivity testing at different incident angles. In addition, a simple transmission testing system is set up and used as shown in Fig. 9(c). Two horn antennas are placed opposite to each other, with a rotatable absorption screen in the middle. By obtaining the transmission coefficient

TABLE 2. Comparisons between our proposed design and other published absorber works for wide-angle applications.

Ref.	Angular stability			Absorption performance			Element structure		
	Predictable	Usable angle	Min. AR (70°)	Synthesis	FBW (0°)	FBW (70°)	Substrate layer	Resistor	Profile (λ_L)
[5]	No	0°~75°	50% (75°)*	No	101.1%	-	3	-	0.33
[9]	No	0°~75°	55% (75°)*	No	192.9%	192.9% (75°)	5	-	0.16
[14]	No	0°~65°	-	No	85.8%	-	3	18	0.18
[15]	No	0°~70°	69%	No	61%	48.5%	6	8	0.09
[18]	Yes	50°~80°	90% (75°)	No	-	61.2% (75°)	1	4	0.33
[22]	No	0°~75°	70% (75°)	No	76.9%	76.9% (75°)	-	-	0.16
Prop.	**Yes**	**0°~70°**	**82%**	**Yes**	**128.83%**	**103.95%**	**1**	**1**	**0.22**

λ_L is the wavelength at the lowest frequency in free space.
* means data extracted from the original figures.

between two horns, the electromagnetic properties of the fabricated prototype can be gained. During the measurement, the far-field condition in [30] and calibration method in [31] are taken into account for better measurement accuracy.

The comparisons between synthetizations, simulations, and measurements are shown in Fig. 10 to Fig. 12. Acceptable agreement can be observed in these results. The main reasons for result deviation can be attributed to discontinuities between different TLs, additional losses from manufacturing, and measurement errors. For normal incidence in Fig. 10, the synthesized, simulated, and measured bandwidths (absorption ratio larger than 80%) are 116.25% (from 3.35 to 12.65GHz), 114.11% (from 3.5 to 12.8GHz), and 128.83% (from 2.9 to 13.4GHz). Herein, the absorption ratio (AR) can be derived as [23]. The average in-band ARs are 92.1%, 91.0, and 93.5%, respectively. The undesired reflections ($|S_{11,co.}|$ and $|S_{11,cro.}|$) and transmissions ($|S_{21,co.}|$ and $|S_{21,cro.}|$) are lower than −7dB, leading to high in-band ARs with low energy leakage and polarization conversion. With regard to 45° oblique incidence, operating bandwidths of 113.75% (average AR of 97.2%), 114.81% (average AR of 95.0%), and 120% (average AR of 92.9%) are realized by synthetizations, simulations, and measurements. As to the larger incident angle of 70°, synthesized, simulated, and measured show bandwidths of 106.25% (average AR of 91.3%), 106.17% (average AR of 90.0%), and 103.95% (average AR of 92.0%). Within the specific C-band and X-band, the average (minimum) measured ARs under normal, 45°, and 70° incidence are 94.2% (88.4%), 94.0% (81.5%), and 92.3% (82.0%). The above performances are summarized in Table 1. From these results, the proposed design method can be indeed utilized to obtain the microwave absorber with 70° angular stability.

In order to further demonstrate the advantages of our work in terms of important performance, Table 2 shows the detailed comparisons between the proposed design and

$$
\begin{cases}
k_1 = \frac{[(z_2+z_c)z_d+z_2z_c][(z_b+z_1)z_a+z_bz_1](z_Rz_{\text{in}}-z_az_d)(z_1+z_2)}{2\sqrt{z_Rz_{\text{in}}z_az_bz_1z_2z_cz_d}} \\
k_2 = \frac{(z_Rz_a-z_{\text{in}}z_d)[(z_2+z_c)z_d+z_2z_c][(z_b+z_1)z_a+z_bz_1](z_1+z_2)}{2\sqrt{z_Rz_{\text{in}}z_az_bz_1z_2z_cz_d}} \\
k_3 = \frac{1}{2\sqrt{z_Rz_{\text{in}}z_az_bz_1z_2z_cz_d}}\Big\{\Big[\big((z_2+2z_c)z_1{}^2+\big(z_2{}^2+(z_b+z_c)z_2+2z_bz_c\big)z_1+2z_bz_c(z_2+z_c)\big)z_d\Big] \\
\quad +\big(z_1{}^2+(z_b+z_2)z_1+2z_bz_2\big)z_2z_cz_a{}^2z_d \\
\quad +\Big[\big((z_2+2z_c)z_1+(z_2+z_c)z_2\big)z_bz_1z_d{}^2+\big(-(z_Rz_{\text{in}}-z_bz_2)z_1{}^2z_c-\big(z_Rz_{\text{in}}-z_2{}^2\big)z_bz_1z_c-(z_2+z_c)z_bz_2z_Rz_{\text{in}}\big)z_d\Big] \\
\quad -\big(z_1{}^2+(z_b+z_2)z_1+2z_bz_2\big)z_2z_cz_Rz_{\text{in}}z_a \\
\quad -2\Big[\Big(\big(\tfrac{z_2}{2}+z_c\big)+\tfrac{(z_2+z_c)z_2}{2}\Big)z_d+(z_1+z_2)z_2z_c\Big]z_bz_1z_Rz_{\text{in}}\Big\} \\
k_4 = \frac{1}{2\sqrt{z_Rz_{\text{in}}z_az_bz_1z_2z_cz_d}}\Big\{-\Big[\big(z_1{}^2z_c+z_bz_1z_c+(z_2+z_c)z_bz_2\big)z_d+\big(z_1{}^2+(z_b+z_2)z_1+2z_bz_2\big)z_2z_c\Big]z_a{}^2z_R \\
\quad +\Big[-\big(z_1{}^2z_c+z_bz_1z_c+(z_2+z_c)z_bz_2\big)z_d{}^2z_{\text{in}}+\big(z_Rz_1{}^2-z_{\text{in}}z_2{}^2\big)z_bz_cz_d+(z_1+z_2)z_Rz_bz_1z_2z_c\Big]z_a \\
\quad -[((z_2+2z_c)z_1+(z_2+z_c)z_2)z_d+(z_1+z_2)z_Rz_bz_1z_2z_cz_d] \\
k_5 = \frac{-\big[\big(z_1{}^2z_c+z_bz_1z_c+(z_2+z_c)z_bz_2\big)z_d+z_bz_2{}^2z_c\big]z_a{}^2z_d+\big(z_Rz_{\text{in}}z_2{}^2-z_1{}^2z_d{}^2\big)z_az_bz_c+[z_1z_d+((z_1+z_2)z_2)]z_Rz_{\text{in}}z_bz_1z_c}{2\sqrt{z_Rz_{\text{in}}z_az_bz_1z_2z_cz_d}} \\
k_6 = \frac{\big(z_Rz_a{}^2z_2{}^2-z_{\text{in}}z_1{}^2z_c{}^2\big)z_bz_c}{2\sqrt{z_Rz_{\text{in}}z_az_bz_1z_2z_cz_d}}
\end{cases}
\tag{A-1}
$$

other published absorber works for wide-angle applications. Compared with [5], [9], [14], [15], and [22], the proposed structure realizes a predictable higher absorption ratio under a large angle. The structure in [18] achieves high efficiencies under large angles, however, the usable angle and fractional bandwidth are narrower than our design. In addition, our work is synthesized and obtained with a single-layered substrate and a single resistor. According to the above comparison, it is clear that the proposed absorber design in this article accomplishes a predictable and stable high efficiency within a large angle range under a simple structure.

IV. CONCLUSION

In this article, the synthesis and design of 3-D microwave absorber with large angular stability for specific C-band and X-band have been presented. The operating principle is investigated based on our proposed universal equivalent TL model. The wide-angle performance is successfully improved by selecting a proper synthesized angle. A prototype with 70° angular stability is implemented from theoretical analysis and element design. Within C-band and X-band, the measured average ARs under different incidences are higher than 92.3%. Minimum ARs within the operating bandwidth are larger than 81.5%. In addition to the single-layered structure with only one resistor in each element, this type of absorber can be viewed as a promising candidate for wide-angle absorption applications.

APPENDIX

The coefficients of k_1–k_6 are detailly given in (A-1) shown at the bottom of the previous page.

ACKNOWLEDGMENT

The authors would like to appreciate Associate Prof. Ning Liu, Hao-Ran Fu, and Li-Ning Xu in Dalian University of Technology for their kind support in measurements.

REFERENCES

[1] W. Emerson, "Electromagnetic wave absorbers and anechoic chambers through the years," *IEEE Trans. Antennas Propag.*, vol. 21, no. 4, pp. 484–490, Jul. 1973.

[2] J. Chen et al., "High-impedance surface-based broadband absorbers with interference theory," *IEEE Trans. Antennas Propag.*, vol. 63, no. 10, pp. 4367–4374, Oct. 2015.

[3] H. Chen, W.-B. Lu, Z.-G. Liu, J. Zhang, A.-Q. Zhang, and B. Wu, "Experimental demonstration of microwave absorber using large-area multilayer graphene-based frequency selective surface," *IEEE Trans. Microw. Theory Techn.*, vol. 66, no. 8, pp. 3807–3816, Aug. 2018.

[4] Y.-T. Zhao, B. Chen, and B. Wu, "Miniaturized periodicity broadband absorber with via-based hybrid metal-graphene structure for large-angle RCS reduction," *IEEE Trans. Antennas Propag.*, vol. 70, no. 4, pp. 2832–2840, Apr. 2022.

[5] J. Xie et al., "Truly all-dielectric ultrabroadband metamaterial absorber: Water-based and ground-free," *IEEE Antennas Wireless Propag. Lett.*, vol. 18, pp. 536–540, 2019.

[6] W. Li, X. Chen, Z. Zhang, Z. Wu, L. Yang, and Y. Zou, "Ultralight and low-cost structural absorbers with enhanced microwave absorption performance based on sustainable waste biomass," *IEEE Trans. Antennas Propag.*, vol. 70, no. 1, pp. 401–409, Jan. 2022.

[7] Y, Xi, W. Jiang, K. Wei, T. Hong, and S. Gong, "An optically transparent hybrid mechanism metasurface for wideband, wide-angle and omnidirectional scattering suppression," *IEEE Trans. Antennas Propag.*, vol. 71, no. 1, pp. 422–432, Jan. 2023.

[8] Z. Sun, L. Yan, X. Zhao, and R. X.-K. Gao, "An ultrawideband frequency selective surface absorber with high polarization-independent angular stability," *IEEE Antennas Wireless Propag. Lett.*, vol. 22, no. 4, pp. 789–793, Apr. 2023.

[9] Z.-C. Lin, Y. Zhang, L. Li, Y.-T. Zhao, J. Chen, and K.-D. Xu, "Extremely wideband metamaterial absorber using spatial lossy transmission lines and resistively loaded high impedance surface," *IEEE Trans. Microw. Theory Techn.*, vol. 71, no. 8, pp. 3323–3332, Aug. 2023.

[10] A. Dhumal, M. S. Bisht, A. Bhardwaj, M. Saikia, S. Malik, and K. V. Srivastava, "Screen printed polarization independent microwave absorber for wideband RCS reduction," *IEEE Trans. Electromagn. Compat.*, vol. 65, no. 1, pp. 96–103, Feb. 2023.

[11] S. Soghi, H. Heidar, M. R. Haraty, and V. Nayyeri, "Single-layer broadband optically transparent metamaterial absorber using gold thin film," *IEEE Trans. Microw. Theory Techn.*, early access, Nov. 16, 2023, doi: 10.1109/TMTT.2023.3331018.

[12] S. Pandit, Y. Youn, D. Kim, D. An, and W. Hong, "Polarization- and incident-angle independent wideband microwave absorber using ruthenium oxide on a single-layer LTCC substrate," *IEEE Trans. Electromagn. Compat.*, vol. 66, no. 1, pp. 161–168, Feb. 2024.

[13] A. Ghaneizadeh, M. Joodaki, J. Borcsok, A. Golmakani, and K. Mafinezhad, "Analysis, design, and implementation of a new extremely ultrathin 2-D-isotropic flexible energy harvester using symmetric patch FSS," *IEEE Trans. Microw. Theory Techn.*, vol. 68, no. 6, pp. 2108–2115, Jun. 2020.

[14] J. Yu, W. Jiang, and S. Gong, "Wideband angular stable absorber based on spoof surface plasmon polariton for RCS reduction," *IEEE Antennas Wireless Propag. Lett.*, vol. 19, pp. 1058–1062, 2020.

[15] T. Shi, L. Jin, L. Han, M.-C. Tang, H.-X. Xu, and C.-W. Qiu, "Dispersion-engineered, broadband, wide-angle, polarization-independent microwave metamaterial absorber," *IEEE Trans. Antennas Propag.*, vol. 69, no. 1, pp. 229–238, Jan. 2021.

[16] S. C. Bakshi, D. Mitra, and F. L. Teixeira, "Wide-angle broadband rasorber for switchable and conformal application," *IEEE Trans. Microw. Theory Techn.*, vol. 69, no. 2, pp. 1205–1216, Feb. 2021.

[17] Z. Cao et al., "Impedance well effect from circuit analysis and new design concepts for ultrabroadband passive absorber," *IEEE Trans. Antennas Propag.*, vol. 70, no. 10, pp. 9942–9946, Oct. 2022.

[18] Q. Lv et al., "Wideband dual-polarized microwave absorber at extremely oblique incidence," *IEEE Trans. Antennas Propag.*, vol. 71, no. 3, pp. 2497–2506, Mar. 2023.

[19] V. P. Inbavalli, V. P. Sakthivel, C. Venkatesh, and T. R. S. Kumar, "Design of broadband circuit analog absorber with optimal thickness for stable angular response in C, X, Ku, and K bands," *IEEE Trans. Electromagn. Compat.*, vol. 65, no. 6, pp. 2065–2069, Dec. 2023.

[20] H. Jiang et al., "A conformal metamaterial-based optically transparent microwave absorber with high angular stability," *IEEE Antennas Wireless Propag. Lett.*, vol. 20, no. 8, pp. 1399–1403, Aug. 2021.

[21] Z. Zhu et al., "Origami-based metamaterials for dynamic control of wide-angle absorption in a reconfigurable manner," *IEEE Trans. Antennas Propag.*, vol. 70, no. 6, pp. 4558–4568, Jun. 2022.

[22] J. Yadav, M. Saikia, K. V. Srivastava, and J. Ramkumar, "Three-dimensional rotation of FSS unit cell in broadband microwave absorber for large oblique incidence response," *IEEE Trans. Electromagn. Compat.*, vol. 65, no. 5, pp. 1320–1328, Oct. 2023.

[23] T.-X. Feng and L. Zhu, "Ultra-wideband 3-D microwave absorbers with composite slotlines and microstrip lines: Synthetic design and implementation," *IEEE Open J. Antennas Propag.*, vol. 4, pp. 303–311, 2023.

[24] T.-X. Feng and L. Zhu, "Designs of 3-D microwave absorbers with synthesizable absorptive performances," *IEEE Trans. Electromagn. Compat.*, vol. 66, no. 1, pp. 80–87, Feb. 2024.

[25] H. J. Carlin and W. Kohler, "Direct synthesis of band-pass transmission line structures," *IEEE Trans. Microw. Theory Techn.*, vol. 13, no. 3, pp. 283–297, May 1965.

[26] L. Zhu, S. Sun, and R. Li, *Microwave Bandpass Filters for Wideband Communications*. Hoboken, NJ, USA: Wiley, 2012.

[27] Q.-S. Wu and L. Zhu, "Wideband impedance transformers on parallel-coupled and multisection microstrip lines: Synthesis design and implementation," *IEEE Trans. Compon., Packag., Manuf. Technol.*, vol. 6, no. 12, pp. 1873–1880, Dec. 2016.
[28] J. A. Kong, *Electromagnetic Wave Theory*. New York, NY, USA: Wiley, 1986.
[29] L. Zhang, H. Lu, P. Zhou, J. Xie, and L. Deng, "Oblique incidence performance of microwave absorbers based on magnetic polymer composites," *IEEE Trans. Magn.*, vol. 51, no. 11, pp. 1–4, Nov. 2015.
[30] C. A. Balanis, *Antenna Theory Analysis and Design*, 3rd ed. New York, NY, USA: Wiley, 2005.
[31] M. Al-Joumayly and N. Behdad, "A new technique for design of low-profile, second-order, bandpass frequency selective surfaces," *IEEE Trans. Antennas Propag.*, vol. 57, no. 2, pp. 452–459, Feb. 2009.

TIAN-XI FENG (Member, IEEE) was born in Yichun, Heilongjiang, China, in 1994. He received the B.S. degree in electronic information science and technology and the M.Eng. degree in electromagnetic field and microwave technology from Xidian University, Xi'an, China, in 2017 and 2020, respectively, and the Ph.D. degree in electrical and computer engineering from the University of Macau, Macau, China, in January 2024.

Since December 2023, he is an Assistant Professor with the School of Information and Communication Engineering, Dalian University of Technology, Dalian, China. His research interests include electromagnetic manipulation structures, antenna arrays, and 3-D microwave absorbers.

Mr. Feng was the recipient of the Honorable Mention Award from the 35th International Union of Radio Science General Assembly and Scientific Symposium in 2023. He is currently serving as a Reviewer for IEEE ANTENNAS AND WIRELESS PROPAGATION LETTERS and *IET Microwaves, Antennas & Propagation*.

LEI ZHU (Fellow, IEEE) received the B.Eng. and M.Eng. degrees in radio engineering from the Nanjing Institute of Technology (currently Southeast University), Nanjing, China, in 1985 and 1988, respectively, and the Ph.D. degree in electronic engineering from the University of Electro-Communications, Tokyo, Japan, in 1993.

From 1993 to 1996, he was a Research Engineer with Matsushita-Kotobuki Electronics Industries Ltd., Tokyo. From 1996 to 2000, he was a Research Fellow with the École Polytechnique de Montréal, Montréal, QC, Canada. From 2000 to 2013, he was an Associate Professor with the School of Electrical and Electronic Engineering, Nanyang Technological University, Singapore. He joined as a Full Professor with the Faculty of Science and Technology, University of Macau, Macau, China, in August 2013. He was promoted as a Distinguished Professor in December 2016, and then as a Chair Professor in October 2023. From August 2014 to August 2017, he served as the Head of Department of Electrical and Computer Engineering, University of Macau. So far, he has authored or coauthored more than 830 papers in international journals and conference proceedings. His papers have been cited more than 16,800 times with the H-index of 64 (source: Scopus). His research interests include microwave circuits, antennas, periodic structures, transmitting/reflecting surfaces, and computational electromagnetics.

Dr. Zhu was the recipient of the 1997 Asia–Pacific Microwave Prize Award, the 1996 Silver Award of Excellent Invention from Matsushita-Kotobuki Electronics Industries Ltd., the 1993 Achievement Award in Science and Technology (First Prize) from the National Education Committee of China, the 2020 FST Research Excellence Award from the University of Macau, the 2020 and 2022 Macao Natural Science Awards (Second Prize) from the Science and Technology Development Fund, Macau, and the 2024 IEEE MTT-S Microwave Application Award. He was an Associate Editors of the IEEE TRANSACTIONS ON MICROWAVE THEORY AND TECHNIQUES from 2010 to 2013 and IEEE MICROWAVE AND WIRELESS COMPONENTS LETTERS from 2006 to 2012. He served as a General Chair of the 2008 IEEE MTT-S International Microwave Workshop Series on the Art of Miniaturizing RF and Microwave Passive Components, Chengdu, China, and a Technical Program Committee Co-Chair of the 2009 Asia–Pacific Microwave Conference, Singapore. He served as the member of IEEE MTT-S Fellow Evaluation Committee from 2013 to 2015, and the member of IEEE AP-S Fellows Committee from 2015 to 2017.

HUI LI (Senior Member, IEEE) received the Ph.D. degree in electrical engineering from the Royal Institute of Technology (KTH), Sweden, in 2012.

From 2012 to 2015, she was a Postdoctoral Researcher with the Department of Electrical and Information Technology, Lund University. In 2015, she joined the Dalian University of Technology, where she is currently a Professor. Her current research interests include terminal antennas, wearable antennas, theory of characteristic mode, RFID antennas, antenna-user interactions, millimeter wave antennas, and microwave imaging. She won CST University Publication Award in 2013, the IEEE Women in NEMO for MAPE Award in 2020, and the ACES Women Scientist Award in 2023. She is an Associate Editor of IEEE ANTENNA AND WIRELESS PROPAGATION LETTERS. She is elected as the 2023 IEEE APS Young Professional Ambassador. She is also a member of the Education Committee within the IEEE Antennas and Propagation Society (AP-S), where she has served as the final judge for IEEE AP-S Student Design Contest.